Pergamon

Acta Materialia 50 (2002) 183–193

Acta MATERIALIA

www.elsevier.com/locate/actamat

Rapid solidification behavior of Zn-rich Zn–Ag peritectic alloys

W. Xu [1], Y.P. Feng [2], Y. Li [1,*], G.D. Zhang [3], Z.Y. Li [3]

[1]*Department of Materials Science, National University of Singapore, Singapore 119260*
[2]*Department of Physics, National University of Singapore, Singapore 119260*
[3]*Department of Materials Science and Engineering, Huazhong University of Science and Technology, Wuhan 430074, People's Republic of China*

Received 29 January 2001; accepted 10 August 2001

Abstract

Rapid solidification experiments, including laser remelting, melt-spinning and wedge casting, were carried out to investigate the rapid solidification behavior of Zn-rich Zn–Ag peritectic alloys containing up to 9.0 at% Ag. For comparison, Bridgman solidification experiments of the same alloys were also carried out for growth velocities ranging from 0.02 to 4.82 mm/s, which were lower than that of 12–54.5 mm/s for laser remelting and that in the order of 10^2 mm/s for melt-spun samples. Optical images and transmission electron microscopy (TEM) showed that instead of the typical structure consisting of primary dendrites of ϵ surrounded by peritectic η, a two-phase plate-like $\eta+\epsilon$ with (or without) primary dendrites of ϵ was observed in Zn–3.1, 4.4, 6.3 and 9.0 at% Ag alloys when the growth velocity was higher than a critical value. It was found that the higher was the alloy concentration, the higher was the critical growth velocity for the formation of fully two-phase plate-like $\eta + \epsilon$. From the TEM micrographs, the volume fraction of ϵ in the fully two-phase plate-like $\eta + \epsilon$ increased from 0.09 to 0.50 with increase in alloy concentration from 3.1 to 6.3 at% Ag. A plausible analysis was proposed to interpret the dependence of microstructural transitions on the growth velocity in Zn–3.1 to 9.0 at% Ag alloys, that is, primary dendrites of ϵ in a matrix of peritectic $\eta\rightarrow$two-phase plate-like $\eta + \epsilon$ with primary dendrites of $\epsilon\rightarrow$ fully two-phase plate-like $\eta + \epsilon$.

Keywords: Zn–Ag alloys; Phase transformations; Microstructure; Peritectic; Rapid solidification

1. Introduction

Peritectics are found in many materials such as steels, copper alloys, permanent magnetic materials Co–Sm–Cu [1] and Nd–Fe–B [2], and high T_c superconducting $YBa_2Cu_3O_y$ [3], in which one solid phase reacts with a liquid phase on cooling to produce a second solid phase [4]. Most of the previous investigations on peritectic solidification were focused on equilibrium or near equilibrium solidification behavior, including nucleation [5], peritectic reaction [6], coupled growth [7–9], banded structure [10], solute segregation [11], and

* Corresponding author. Tel.: +65-8743348; fax: +65-7763604.
E-mail address: masliy@nus.edu.sg (Y. Li).

1359-6454/02/$22.00
PII: S1359-6454(01)00321-4

phase selection [12]. However, understanding of the rapid solidification behavior of peritectic alloys is still limited because of the complexity of the peritectic reaction under non-equilibrium conditions, which results in the formation of complex microstructures.

The typical microstructure from peritectic solidification consists of a primary phase surrounded by a peritectic phase formed via the peritectic reaction. However, varying solidification conditions and alloy compositions lead to distinct morphologies, such as banded and cellular structures of primary and peritectic phases in Sn–Cd peritectic alloys [13], two-phase plate-like structure in Zn–Cu [14] and coupled growth of primary and peritectic phases in Ni–Al [7], Ti–Al [8], Fe–Ni [9] and Zn–Ag [15] peritectic systems. Coupled growth of two phases and the formation of banded structure in peritectic systems have recently drawn much attention [4]. Coupled growth of two phases with a planar liquid/solid interface was suggested to occur in peritectic systems close to the peritectic temperature [16,17]. However, experimental attempts to achieve two-phase coupled growth in peritectic alloys grown at velocities close to the limit of the constitutional supercooling, have failed except for studies on Ni–Al [7], Ti–Al [8] and Fe–Ni [9]. The reason was ascribed to some extent to experimental difficulties in Bridgman growth at the extremely low velocities involved [9].

It is possible that coupled growth of two phases in peritectic alloys might occur, however, when the growth velocity is high enough to suppress the formation of the primary phase and to ensure a planar liquid/solid growth interface [16,17]. Our previous attempt [15] reported the formation of a two-phase eutectic-like lamellar structure in as-spun ribbons of a Zn–6.3 at% Ag peritectic alloy processed by the melt spinning technique. Subsequently, systematic experiments were carried out using several rapid solidification techniques, that is, laser remelting, melt spinning and wedge casting. The main purpose of the present study is to investigate the rapid solidification behavior of Zn-rich Zn–Ag peritectic alloys, in order to gain more insight into the non-equilibrium formation of coupled growth in peritectic systems. In addition, results of Bridgman solidification were also provided for comparison.

2. Experimental

Seven Zn–Ag alloys containing up to 9.0 at% Ag were prepared by melting pure 99.99% Zn and pure 99.99% Ag in air in an induction furnace. Specimens with 30×50×8 mm (width×length×thickness) and compositions between 0.6 and 9.0 at% Ag were prepared for laser remelting experiments. Before laser treatment, the specimens were ground on 1000 grit SiC paper to ensure a similar surface quality for each specimen as well as to enhance absorption of the laser beam. The laser remelting experiments were carried out using a continuous wave 1.0 kW CO_2 laser at beam scanning velocities ranging from 16.7 to 120 mm/s. A normally incident laser beam was focused to a spot diameter of 1.0 mm and had a power density of 3.2×10^4 W/cm^2. During the laser treatments, a continuous flow of argon was blown onto the surface in order to reduce heavy oxidation of the molten pool. Some 6–7 g of the as-cast ingot of Zn–6.3 at% Ag was melt-spun under argon from a quartz crucible on to a copper wheel at a speed of 20 m/s. Samples of the melt were cast into rods 1.1 or 2.5 mm diameter and 100 mm long by vacuum injection into quartz tubes. Rods were remelted for Bridgman solidification at withdrawal velocities ranging from 0.02 to 0.48 mm/s for those with diameter 2.5 mm and from 0.75 to 4.82 mm/s for those with diameter 1.1 mm. The operative temperature gradient during unidirectional solidification was 15 K/mm. Other samples of melts with compositions between 0.6 and 9.0 at% Ag were cast into a wedge-section copper mould (wedge angle 5°) of wall thickness 50 mm, width 50 mm and height 102 mm, giving wedge castings increasing in section from 0.1 mm at the bottom to 9 mm at the top. Longitudinal and transverse sections of laser remelted, melt-spun, Bridgman, and wedge cast samples for optical and scanning electron microscopic studies were prepared by conventional mechanical grinding, polishing and chemical etching in a diluted 1 vol% nitric acid solution. Transmission electron microscopic (TEM) studies were carried out on sections parallel to and close to the surface of laser remelted specimens and on the section parallel to the ribbon plane of Zn–6.3 at% Ag as-spun ribbons.

The Zn-rich Zn–Ag binary phase diagram is redrawn from Ref. [18] and shown in Fig. 1, in which a peritectic reaction, $\epsilon + L \rightarrow \eta$, occurs at a temperature of 431°C. Phase ϵ ($AgZn_3$) is termed the primary phase and η (Zn-rich solid solution) the peritectic phase. The compositions of liquid, primary and peritectic phases in peritectic equilibrium are referred to as C_L, C_ϵ and C_η, respectively.

3. Results

3.1. Typical microstructures and microstructural transitions

In this section, the results will be reported in the sequence laser remelting and melt spinning, Bridgman solidification, and wedge casting. The microstructures formed in the present study are identified below for reference:

1. C_η^R or C_η^P: single-phase regular or plate-like cellular η.
2. D_η^C: cellular dendrites of η.
3. $D_\epsilon^E D_\eta^C$: cellular dendrites of η with primary dendrites of ϵ.
4. $D_\epsilon^E C_{\eta\epsilon}^P$: two-phase plate-like $\eta + \epsilon$ with primary dendrites of ϵ.
5. $C_{\eta\epsilon}^P$: fully two-phase plate-like $\eta + \epsilon$.
6. $D_\epsilon M_\eta$: primary dendrites of ϵ in a matrix of η.

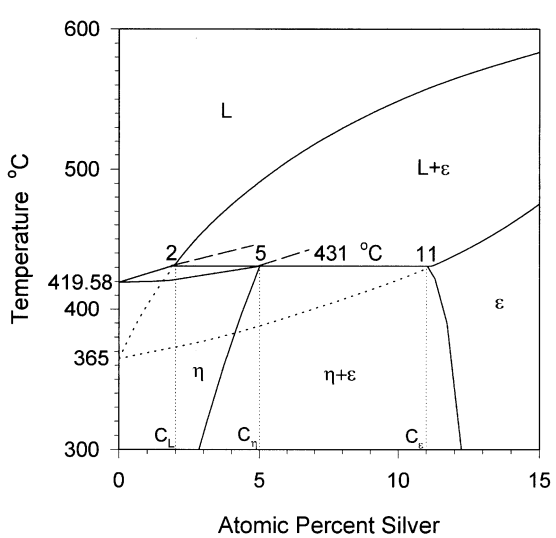

Fig. 1. Binary equilibrium phase diagram of Zn-rich Zn–Ag alloys (Redrawn from Ref. [18]). Dashed lines indicates the metastable extension of liquidus and solidus lines.

3.1.1. Laser remelted and melt-spun samples

Three distinct types of solidification microstructures, namely, single-phase plate-like cellular $\eta(C_\eta^P)$, two-phase plate-like $\eta + \epsilon$ with primary dendrites of $\epsilon(D_\epsilon^E C_{\eta\epsilon}^P)$ and fully two-phase plate-like $\eta+\epsilon$ ($C_{\eta\epsilon}^P$), were identified in laser remelted samples. A single-phase plate-like cellular η with a finer spacing formed in 0.6 and 1.8 at% Ag alloys, as shown in Fig. 2(a). For 3.1 and 4.4 at% Ag alloys, with increasing growth velocity or laser beam scanning velocity, the volume fraction of primary ϵ dendrites decreased and a fully two-phase plate-like $\eta + \epsilon$ [Fig. 3(a)] dominated when the growth velocity exceeded 43.6 mm/s for 3.1 at% Ag and 54.5 mm/s for 4.4 at% Ag. In addition, for laser remelted Zn–6.3 and 9.0 at% Ag alloys, instead of the typical microstructure consisting of primary dendritic ϵ in a matrix of peritectic $\eta(D_\epsilon M_\eta)$, a structure of two-phase plate-like $\eta + \epsilon$ with primary dendrites of $\epsilon(D_\epsilon^E C_{\eta\epsilon}^P)$ [Fig. 4(a)] was observed.

The melt-spinning technique was employed on the Zn–6.3 at% Ag alloy to investigate the microstructure of this alloy at a much high growth velocity. The results for melt-spun Zn–6.3 at% Ag were reported in a previous paper [15]. As expected, in the as-spun ribbons, fully two-phase plate-like (or lamellar) $\eta + \epsilon$ colonies were embedded in a matrix of the degenerate lamellae (Fig. 5). The growth velocity in the as-spun ribbons was estimated to be in the order of 10^2 mm/s [19], which is much higher than the applied growth velocity in laser remelting in the present study.

3.1.2. TEM morphological study on laser remelted and melt-spun samples

TEM studies were carried out on samples with single-phase plate-like η or fully (or nearly fully) two-phase plate-like $\eta + \epsilon$, such as laser remelted samples grown at 43.5 mm/s for 0.6, 1.8, 3.1 and 4.4 at% Ag alloys and melt-spun ribbons for 6.3 at% Ag alloy. TEM micrographs with selected-area diffraction patterns provided evidence for the for-

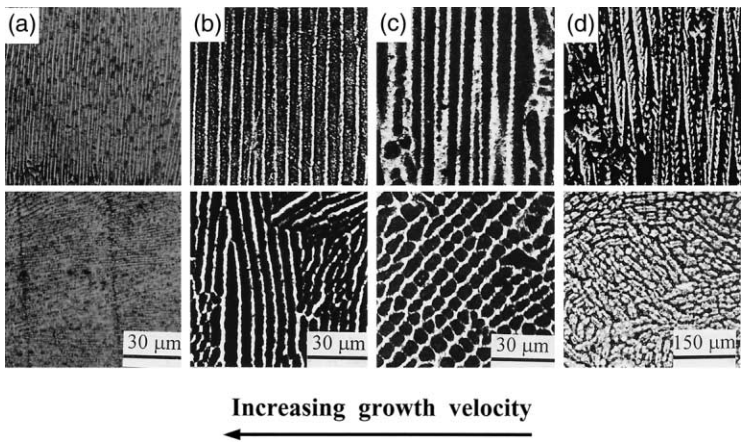

Fig. 2. Optical micrographs showing microstructure evolution with variation of growth velocity for Zn–1.8 at% Ag alloy: (a) finely plate-like cells of η (C_η^{P}) grown at 12 mm/s; (b) plate-like cells of η (C_η^{P}) grown at 3.54 mm/s; (c) regular cells of η (C_η^{R}) grown at 2.06 mm/s; (d) cellular dendrites of η (D_η^{C}) grown at 0.48 mm/s. (a) Laser remelting; (b)–(d) Bridgman solidification. Upper, longitudinal section; lower, transverse section.

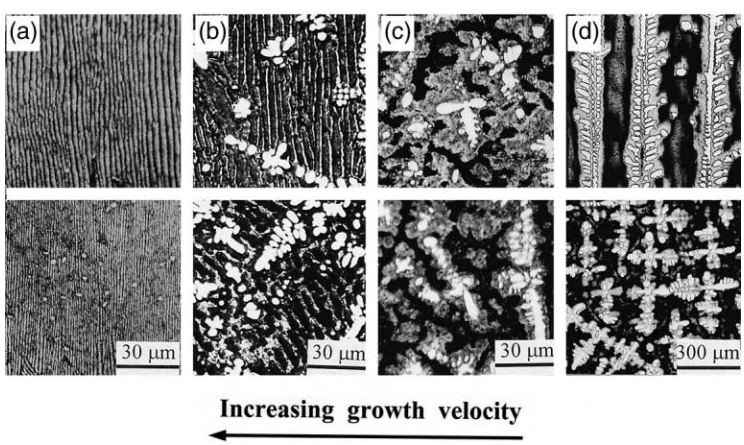

Fig. 3. Optical micrographs showing microstructure evolution with variation of growth velocity for Zn–3.1 at% Ag alloy: (a) nearly fully two-phase plate-like $\eta + \epsilon$ with few primary dendrites of ϵ ($C_{\eta\epsilon}^{\mathrm{P}}$) grown at 43.6 mm/s; (b) two-phase plate-like $\eta + \epsilon$ with primary dendrites of ϵ ($D_\epsilon^{\mathrm{E}} C_{\eta\epsilon}^{\mathrm{P}}$) grown at 4.15 mm/s; (c) non-aligned primary dendrites of ϵ surrounded by η produced by peritectic reaction ($D_\epsilon^{\mathrm{E}} M_\eta^{\mathrm{Pe}}$) grown at 1.52 mm/s; (d) arrayed primary dendrites of ϵ surrounded by η produced by peritectic reaction ($D_\epsilon^{\mathrm{A}} M_\eta^{\mathrm{Pe}}$) grown at 0.045 mm/s. (a) Laser remelting; (b)–(d) Bridgman solidification. Upper, longitudinal section; lower, transverse section.

mation of single-phase cellular η and two-phase plate-like $\eta + \epsilon$, as shown in Fig. 6. Fig. 6(a) shows plate-like cellular η in the transverse section of laser remelted Zn–1.8 at% Ag, with a small amount of intercellular particles due to segregation. Fig. 6(f) is the selected-area diffraction pattern of Fig. 6(a) in a field including cells and intercellular boundaries, showing only the η phase present. With an increase in concentration to 3.1 and 4.4 at% Ag, a two-phase plate-like structure formed as shown in Figs. 6(b) and (c). The corresponding selected-area diffraction patterns [Figs. 6(g) and (h)] indicated that both η and ϵ phases were present. Fig. 6(d) shows a bright-field image of 6.3

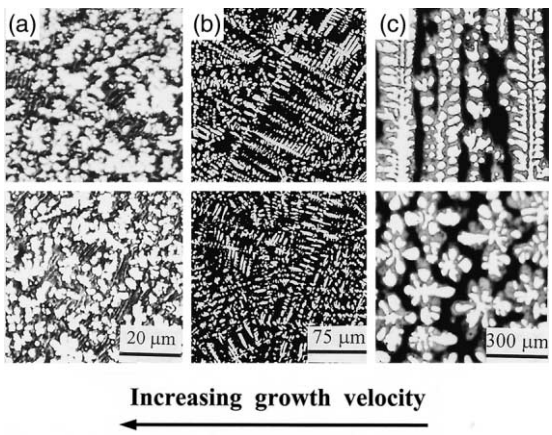

Fig. 4. Optical micrographs showing microstructure evolution with variation of growth velocity for Zn–6.3 at% Ag alloy: (a) two-phase plate-like $\eta + \epsilon$ with primary dendrites of ϵ ($D_{\epsilon}^{E}C_{\eta\epsilon}^{P}$) grown at 12 mm/s; (b) non-aligned primary dendrites of ϵ in a matrix of η without peritectic reaction ($D_{\epsilon}^{E}M_{\eta}^{NPe}$) grown at 2.39 mm/s; (c) arrayed primary dendrites of ϵ surrounded by η produced by peritectic reaction ($D_{\epsilon}^{A}M_{\eta}^{Pe}$) grown at 0.02 mm/s. (a) Laser remelting; (b) and (c) Bridgman solidification. Upper, longitudinal section; lower, transverse section.

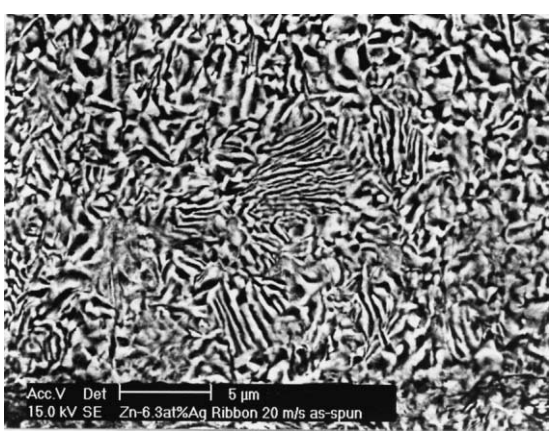

Fig. 5. SEM micrographs of as-spun ribbons of Zn–6.3 at% Ag peritectic alloy, showing two-phase plate-like (lamellar) colonies embedded in a matrix of the degenerate lamellae.

at% Ag as-spun ribbons and Fig. 6(i) the diffraction pattern indicating two phases, whereas Fig. 6(e) is the corresponding dark-field image of η when the η(002) diffraction spot in Fig. 6(i) was selected. From Figs. 6(b)–(d), it was also noted that, with increasing alloy concentration, the volume fraction of ϵ (bright phase) increased from 0.09 for 3.1 at% Ag to 0.26 for 4.4 at% Ag, then to 0.5 for 6.3 at% Ag.

3.1.3. Bridgman solidification

For comparison, Bridgman solidification experiments were also carried out on Zn–0.6, 1.8, 2.5, 3.1, 4.4, 6.3 and 9.0 at% Ag alloys at growth velocities ranging from 0.02 to 4.82 mm/s. Five distinct types of solidification microstructure were identified in the Bridgman samples in terms of the growth morphologies of ϵ and η phases: C_{η}^{R} or C_{η}^{P}; D_{η}^{C}; $D_{\epsilon}^{E}D_{\eta}^{C}$; $D_{\epsilon}^{E}C_{\eta\epsilon}^{P}$; $D_{\epsilon}M_{\eta}$.

For Zn–0.6 and 1.8 at% Ag alloys, two microstructural transitions with increasing growth velocities, namely, cellular dendritic η [Fig. 2(d)] to regular cellular η [Fig. 2 (c)], and then to plate-like cellular η [Fig. 2(b)] were observed in Bridgman samples. As alloy concentration increased to 3.1 and 4.4 at% Ag, two microstructural transitions were also observed in Bridgman samples when the growth velocity increased. They were arrayed primary dendrites of ϵ surrounded by peritectic η [Fig. 3(d)] to non-aligned primary dendrites of ϵ surrounded by peritectic η [Fig. 3(c)] then to a two-phase plate-like η+ϵ with primary dendrites of ϵ [Fig. 3(b)]. On the other hand, Bridgman samples of Zn–6.3 and 9.0 at% Ag alloys showed a microstructural transition from arrayed primary dendrites of ϵ with peritectic η [Fig. 4(c)] to non-aligned primary dendrites of ϵ with (or without) peritectic η [Fig. 4(b)] as the growth velocity increased. The two-phase plate-like η+ϵ with primary dendrites of ϵ was not observed in 6.3 and 9.0 at% Ag alloys at growth velocities ranging from 0.02 to 4.82 mm/s.

It is reasonable to regard the resulting microstructures of laser remelted and melt-spun samples as corresponding to an extension of Bridgman solidification to a higher growth velocity range. Therefore, a solidification microstructure selection diagram was determined over a wide range of growth velocities and alloy compositions, as shown in Fig. 7. Five main regions were designated with respect to the microstructures observed: single-phase regular cellular (or cellular dendritic) η; single-phase plate-like cellular η; primary dendrites of ϵ in a matrix of η; two-phase plate-like $\eta + \epsilon$ with primary dendrites of ϵ, and fully two-phase plate-like $\eta + \epsilon$.

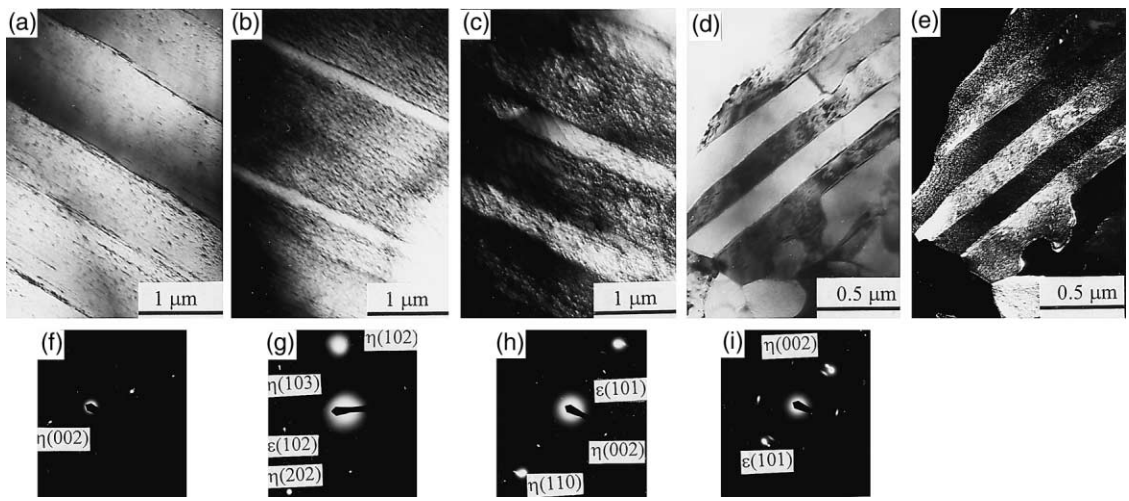

Fig. 6. TEM micrographs of transverse sections. (a) Single-phase plate-like cellular η in Zn–1.8 at% Ag; (b), (c) two-phase plate-like $\eta + \epsilon$ in Zn–3.1 and 4.4 at% Ag respectively; (d), (e) bright and dark-field images of two-phase plate-like $\eta + \epsilon$ in Zn–6.3 at% Ag respectively. (a)–(c) Laser remelted samples grown at 43.6 mm/s. (d) and (e) As-spun ribbons at a wheel speed of 20 m/s, which was reported in our previous paper [15]. (f) Diffraction pattern of (a) including cellular boundaries; (g) diffraction pattern of (b) including two phases; (h) diffraction pattern of (c) including two phases; (i) diffraction pattern of (d) and (e) including two phases.

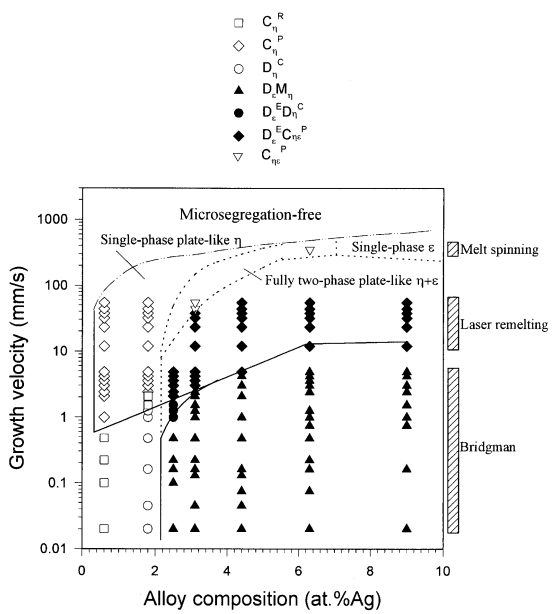

Fig. 7. Microstructure and phase selection map for unidirectional solidification of Zn-rich Zn–Ag peritectic alloys by laser remelting, melt-spining and Bridgman method: ◇, single-phase plate-like cellular η; □, single-phase regular cellular η; ○, cellular dendrites of η; ◆, two-phase plate-like $\eta + \epsilon$ with primary dendrites of ϵ; ●, cellular dendrites of η with primary dendrites of ϵ; ▽, fully two-phase plate-like $\eta + \epsilon$; ▲, primary dendrites of ϵ in a matrix of η.

3.1.4. Wedge casting samples

Besides the techniques discussed above, wedge casting was also employed on present alloys to obtain a range of cooling rates during solidification, so that the range of microstructures linking slowly and more rapidly cooled might be obtained within a single ingot for each alloy composition.

Nine distinct types of solidification microstructure were identified in the wedge-cast samples. They are: D_η^E, equiaxed dendrites of η; D_η^C, cellular dendrites of η; C_η^R or C_η^P, single-phase regular or plate-like cellular η; $D_\epsilon^E M_\eta^{Pe}$, equiaxed primary dendrites of ϵ in a matrix of η with peritectic reaction; $D_\epsilon^E D_\eta^C$, cellular dendrites of η with equiaxed primary dendrites of ϵ; $D_\epsilon^E(C_{\eta\epsilon}^R$ or $C_{\eta\epsilon}^P)$, two-phase regular or plate-like $\eta+\epsilon$ with primary dendrites of ϵ; $C_{\eta\epsilon}^R$ or $C_{\eta\epsilon}^P$, fully two-phase regular or plate-like $\eta + \epsilon$; $D_\epsilon^E M_\eta^{NPe}$, equiaxed primary dendrites of ϵ in a matrix of η without peritectic reaction; $(D_\epsilon^A$ or $C_\epsilon)M_\eta^{NPe}$, cellular dendritic ϵ or cellular ϵ in a matrix of η without peritectic η. The locations of occurrence of these nine microstructures in longitudinal sections of the wedges of the six alloy compositions investigated are shown in Fig. 8, which is in reasonable agreement with that in Fig. 7. It was noted that fully two-phase plate-like or rod-like $\eta + \epsilon$ was only observed in the thinnest

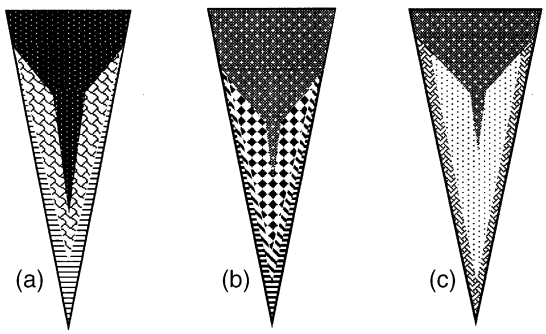

Fig. 8. Schematic diagrams showing the locations of occurrence of the nine principal microstructures in longitudinal sections of wedges for the six alloy compositions investigated: (a) Zn–0.6 and 1.8 at% Ag; (b) Zn–3.1 and 4.4 at% Ag; (c) Zn–6.3 and 9.0 at% Ag. Key: ■, D_η^E; ▨, D_η^C; ▤, $C_\eta^R \vee C_\eta^P$; ▩, $D_\epsilon^E M_\eta^{Pe}$; ◆, $D_\epsilon^E D_\eta^C$; ▨, $D_\epsilon^E(C_{\eta\epsilon}^R$ or $C_{\eta\epsilon}^P)$; ▤, $C_{\eta\epsilon}^R$ or $C_{\eta\epsilon}^P$; ⁘, $D_\epsilon^E M_\eta^{NPe}$; ▨, $(D_\epsilon^A$ or $C_\epsilon)M_\eta^{NPe}$.

region of Zn–3.1 and 4.4 at% Ag wedge cast samples (Fig. 9) as well as laser remelted samples.

3.2. Characteristic length scales of single-phase and two-phase plate-like (or rod-like) structures

The fundamental characteristic length scales, that is, cellular spacing (λ) for single-phase plate-like (or rod-like) cellular structure and interphase spacing (λ_P) for two-phase plate-like (or rod-like) $\eta + \epsilon$, are shown in Fig. 10 as a function of growth velocity and alloy composition, indicating that $\lambda V^{1/2}$ and $\lambda_P V^{1/2}$ are essentially constant for a given composition. Figs. 10(a) and (b) show the measured spacing of single-phase plate-like (or rod-like) cellular η whereas Figs. 10(c)-(f) give the measured spacing of two-phase plate-like (or rod-like) $\eta + \epsilon$ in both Bridgman and laser remelted samples. The value of $\lambda V^{1/2}$ slightly decreases from 330 $\mu m^{3/2}/s^{1/2}$ for 0.6 at% Ag alloy to 315 $\mu m^{3/2}/s^{1/2}$ for 1.8 at% Ag alloy. For λ_P of two-phase plate-like $\eta + \epsilon$ [Figs. 10 (c)–(f)], the value of $\lambda_P V^{1/2}$ decreases from 259 $\mu m^{3/2}/s^{1/2}$ for 3.1 at% Ag alloy to 159 $\mu m^{3/2}/s^{1/2}$ for the 9.0 at% Ag alloy.

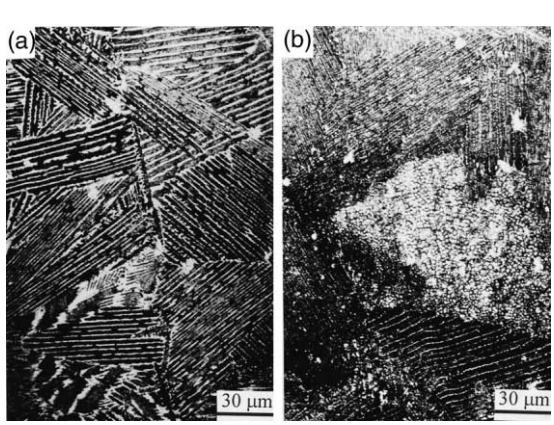

Fig. 9. A fully two-phase plate-like or regular (rod-like) $\eta + \epsilon$ with few primary dendrites of ϵ in a Zn–3.1 at% Ag wedge cast sample. (a) Longitudinal section; (b) transverse section.

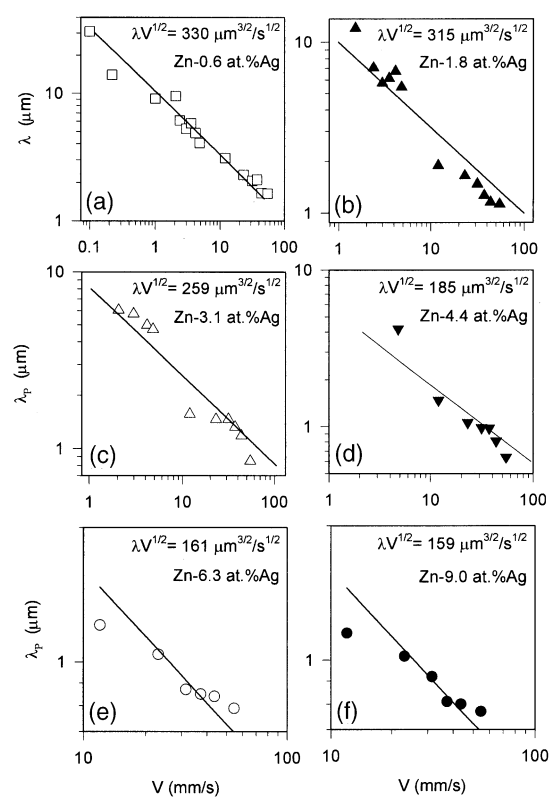

Fig. 10. Intercellular spacing, λ, of cellular η for Zn–0.6 and 1.8 at% Ag, and interphase spacing, λ_P, of two-phase plate-like $\eta + \epsilon$ for Zn–3.1, 4.4, 6.3 and 9.0 at% Ag, as a function of growth velocity. Symbols show experimental data, lines show regression results for the corresponding alloys.

4. Discussion

4.1. Two-phase eutectic-like (plate or rod) structure in peritectic systems

Boettinger [13] carried out experiments on Sn–Cd peritectic alloys and predicted, by an analysis similar to the Jackson–Hunt theory [20] of lamellar eutectic growth, that coupled growth in peritectic systems was unstable. Furthermore and recently, Vandyoussefi et al. [9] pointed out that the classic eutectic growth model could not be directly applied to peritectic coupled growth without modification because the value of a^{L} in the analysis of Boettinger is very sensitive to the exact values of surface energies and of the phase diagram parameters.

On the other hand, Hillert [21] and Laraia and Heuer [22] suggested that a metastable eutectic reaction could occur instead of an equilibrium peritectic reaction in some peritectic systems, particularly those in which the peritectic phase is a compound. The capillary effects associated with fine lamellar structure may lower the liquidus of primary phase and promote a metastable eutectic reaction [22], allowing coupled growth to occur at a temperature below the metastable congruent melting temperature.

In experiments, two-phase plate-like [8,9,14,15] and rod-like [7,13,23] growths have been reported for several peritectic systems. Boettinger [13] and Brody and David [23] observed that at a value of G/V slightly below that determined by constitutional supercooling, two-phase Sn–Cd peritectic alloys solidified with a non-planar interface consisting of cells of α (primary phase) and intercellular β (peritectic phase). Lee and Verhoeven [7] reported two-phase cellular coupled growth of γ and γ' in directional solidification of Ni–Al peritectic alloys at high G/V conditions sufficient to give plane front growth, giving a cell spacing of about 30 μm. Busse and Meissen [8] observed a two-phase plate-like structure with a spacing of 30 μm in TiAl with 53.4 at% Al directionally solidified at a very low growth velocity of 0.83 μm/s. Recently, a eutectic-like lamellar structure was reported in a Fe–4.49 at% Ni peritectic alloy at growth velocities of 10 to 15 μm/s with an interphase spacing of about 80 μm [9] and in a melt-spun Zn–6.3 at% Ag [15] peritectic alloy with a lamellar spacing of 0.36 μm. It should be noted that the observed interphase spacings in the above investigations [7–9,15] are very large, typically one order of magnitude larger than that for eutectic systems at similar growth conditions [9].

However, most of the previous investigations reporting coupled growth in peritectic systems [7–9] were carried out under conditions giving plane front growth, that is, close to the limit of constitutional supercooling. Up to now, no attempts were carried out to study the non-equilibrium effects on the formation of coupled growth in peritectic systems by rapid solidification except for one [15]. In the present study, fully two-phase plate-like $\eta + \epsilon$ was observed in the thinnest region of Zn–3.1 and 4.4 at% Ag wedge cast samples, in the Zn–6.3 at% Ag as-spun ribbons, and also in laser remelted samples when the growth velocity was higher than a critical growth velocity such as 43.5 and 54.5 mm/s for Zn–3.1 and 4.4 at% Ag, respectively. In addition to the fully two-phase plate-like $\eta + \epsilon$, a microstructure consisting of two-phase plate-like $\eta + \epsilon$ with primary dendrites of ϵ was also observed in Zn–3.1, 4.4, 6.3 and 9.0 at% Ag peritectic alloys, which was not reported in Sn–Cd [13,23], Ni–Al [7], Ti–Al [8], or Fe–Ni [9] peritectic systems. It is noted from Figs. 3, 4 and 8 that for the two-phase zone (from 2 to 11 at% Ag), the microstructural evolution with increasing growth velocity, that is, primary dendrites of ϵ in a matrix of $\eta\rightarrow$ two-phase plate-like $\eta + \epsilon$ with primary dendrites of $\epsilon\rightarrow$ fully two-phase plate-like $\eta + \epsilon$, is very similar to those observed in off-eutectic alloys, as shown in Fig. 11. In addition, the critical growth velocity determined by experiments for the formation of fully two-phase plate-like $\eta + \epsilon$ increases with increase in alloy concentration.

In a previous paper [15], from the theory developed by Hillert [21] and Laraia and Heuer [22], it was assumed that there was a conversion of the equilibrium peritectic reaction into a metastable eutectic reaction in the Zn–Ag peritectic system by rapid solidification. It is known that eutectics can be classified as normal and anomalous systems according to the shape of their coupled zone [24]. Therefore, the coupled zone of the metastable eutectic in peritectic systems should have a skewed

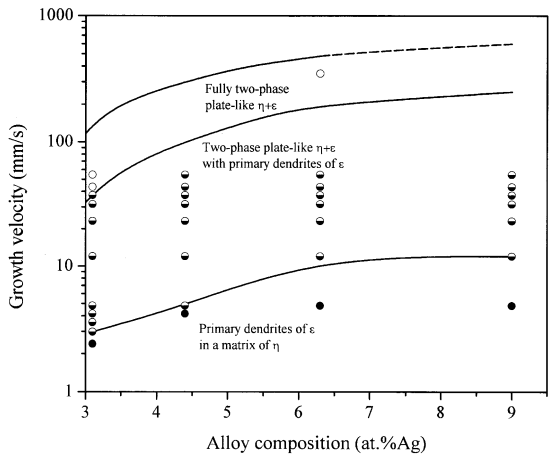

Fig. 11. Experimentally determined microstructure transitions for Zn–3.1 to 9.0 at% Ag alloys as a function of growth velocity and alloy composition, that is, primary dendrites of ϵ in a matrix of $\eta\longrightarrow$ two-phase plate-like $\eta + \epsilon$ with primary dendrites of $\epsilon\longrightarrow$ fully two-phase plate-like $\eta + \epsilon$.

shape due to the large difference between the melting points of two phases. In addition, according to Kerr and Kurz [4], at medium/high growth velocities, the morphology that will be present is the one which has the maximum interface temperature for constrained growth. In the present study, three typical morphologies will be considered, that is, primary dendrites (or cells) of ϵ, two-phase plate-like $\eta + \epsilon$, and primary dendrites (or cells) of η. Determining their growth temperatures could predict which is the dominant morphology at a given growth velocity. Unfortunately, the growth temperature as a function of growth velocity for the two-phase plate-like $\eta + \epsilon$ could not be obtained because the converted metastable eutectic phase diagram in our peritectic system is, as yet, not determined. Instead, using an approach similar to the competitive growth of dendrites and eutectic in anomalous eutectic alloys [24], a plausible analysis will be given below to explain the microstructural transitions with increase in growth velocity for those three morphologies.

Fig. 12 shows a schematic explanation of the microstructural evolution observed in Zn–Ag peritectic alloys with a composition between C_L and C_ϵ. Note that the variations of growth temperatures as a function of growth velocity for the three morphologies, are shown in Fig. 12. For Zn–3.1 at%

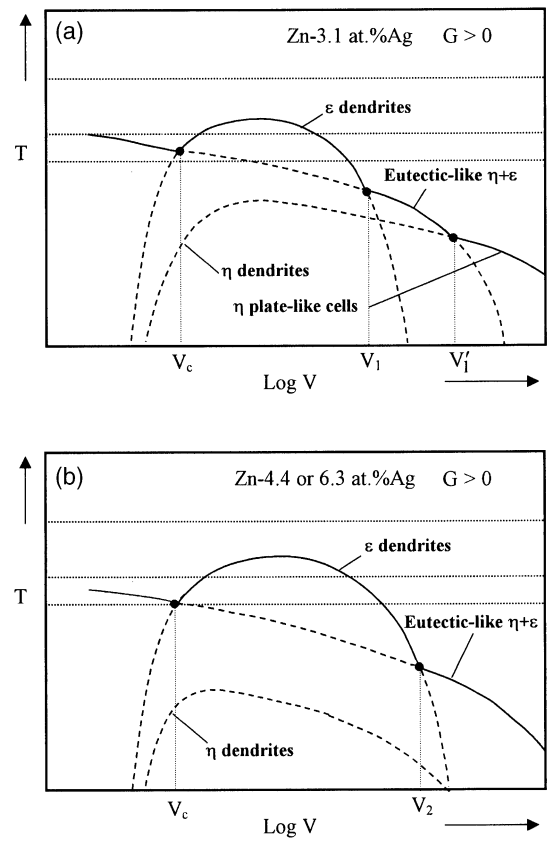

Fig. 12. Plausible interpretation using a method similar to that for anomalous eutectic to show the microstructure evolution of two-phase plate-like $\eta + \epsilon$ observed in Zn–3.1, 4.4 and 6.3 at% Ag alloys.

Ag alloy [Fig. 12(a)], the two-phase plate-like $\eta + \epsilon$ will dominate at a growth velocity (less than V_c) close to the limit of constitutional supercooling although our applied growth velocity is beyond the limit. It was noted that the observations of eutectic-like lamellar two-phase structure in Ni–Al [7], Ti–Al [8] and Fe–Ni [9] should be the result of coupled growth in the range of growth velocity close to V_c. Therefore, the present study could be regarded as the extension of those studies to a higher growth velocity range up to that close to the limit of absolute stability. With increasing growth velocity, the primary dendritic ϵ has a higher growth temperature and becomes the leading phase followed by peritectic η via peritectic reaction. Further increase in growth velocity will firstly

result in the formation of η phase directly from the liquid instead of by peritectic reaction, and then lead the transition from primary ϵ in a matrix of η to two-phase plate-like $\eta + \epsilon$. During this transition, the two morphologies will compete and result in a structure consisting of two-phase plate-like $\eta + \epsilon$ with primary ϵ until the fully two-phase plate-like $\eta + \epsilon$ dominates if the growth velocity is higher than V_1. Finally, if the growth velocity increases to exceed V_1', a single-phase cellular η may be produced rather than two phases, which was not observed in the present Zn–3.1 at% Ag alloy because our applied growth velocity is below V_1'. Fig. 12(b) shows the variations of growth temperature as a function of growth velocity when the alloy concentration increases to Zn–4.4 and 6.3 at% Ag. It was noted from Figs. 11 and 12(b) that increasing alloy concentration increased the critical growth velocity for the formation of fully two-phase plate-like $\eta + \epsilon$ from V_1 to V_2. Therefore, in the present study, the value of the critical velocity is 37.3 mm/s for 3.1 at% Ag and $>$54.5 mm/s for 4.4 at% Ag in laser remelted samples and is in the order of 10^2 mm/s for 6.3 at% Ag in as-spun ribbons [15].

4.2. Characteristic length scales of two-phase plate-like (or rod-like) structure

From Figs. 6 and 10, it was noted that at a given growth velocity of 43.5 mm/s, the interphase spacing for the two-phase plate-like $\eta + \epsilon$ decreased from 1.47 to 1.05 μm when the alloy concentration increased from 3.1 to 4.4 at% Ag. Furthermore, for the Zn–6.3 at% Ag alloy, fully two-phase plate-like $\eta + \epsilon$ formed at a much higher growth velocity (estimated to be in the order of 10^2 mm/s [19]) in the as-spun ribbons, giving an interphase spacing finer than about 0.36 μm as shown in Figs. 6(d) and (e). In addition, the values of $\lambda_P V^{1/2}$ for two-phase plate-like $\eta + \epsilon$ observed in Zn–3.1 to 9.0 at% Ag alloys, that is, 259 to 159 $\mu m^{3/2}/s^{1/2}$, are much higher than that of 9.4 $\mu m^{3/2}/s^{1/2}$ for rapidly solidified hypereutectic Al–Cu alloys [25]. These values of $\lambda_P V^{1/2}$ are also larger than the value of 27 $\mu m^{3/2}/s^{1/2}$ for the Ti–Al [8] peritectic alloy and 45 $\mu m^{3/2}/s^{1/2}$ for Ni–Al [7] peritectic alloys but comparable with that of 252 $\mu m^{3/2}/s^{1/2}$ for the Fe–Ni [9] peritectic alloy.

For peritectic alloys, stable coupled growth has been found for a small volume fraction of the minor phase ($<$0.1) in Ni–Al [7] and Fe–Ni [9] alloys although the volume fraction of the minor phase was reported to be 0.5 for the Ti–Al [8] alloy. In addition, the results for Fe–Ni [9] peritectic alloys also indicated that two-phase growth became unstable when the volume fraction of the minor phase increased. However, in the present study, with increase in alloy concentration, the volume fraction of ϵ in fully two-phase plate-like $\eta+\epsilon$ increased from 0.09 for 3.1 at% Ag to 0.26 for 4.4 at% Ag, then to 0.5 for 6.3 at% Ag. In addition, unlike the results in Fe–Ni [9] peritectic alloy, the two-phase growth of η and ϵ was stable even when the volume fraction of the minor ϵ phase reached 0.5 for the Zn–6.3 at% Ag alloy.

5. Conclusions

Rapid solidification experiments, including laser remelting, melt-spinning and wedge casting, were carried out to investigate the rapid solidification behavior of Zn-rich Zn–Ag peritectic alloys containing up to 9.0 at% Ag. For comparison, Bridgman solidification experiments were also carried out on the same alloys for growth velocities ranging from 0.02 to 4.82 mm/s, which are lower than 12–54.5 mm/s for laser remelted and in the order of 10^2 mm/s for melt-spun samples, thus determining a solidification microstructure selection diagram over a wide range of growth velocities and alloy compositions.

Optical images and TEM showed that a single-phase plate-like cellular η was obtained in Zn–0.6 and 1.8 at% Ag alloys grown at velocities above a critical value, indicating that such a structure was velocity-dependent. However, instead of the typical structure of primary dendrites of ϵ surrounded by peritectic η, a two-phase plate-like $\eta + \epsilon$ with (or without) primary dendrites of ϵ was found in Zn–3.1, 4.4, 6.3 and 9.0 at% Ag alloys when the growth velocity was higher than a critical value. It was found that the higher was the alloy concentration, the higher was the critical growth velocity

for the formation of the fully two-phase plate-like $\eta + \epsilon$. From the TEM micrographs, the volume fraction of ϵ in the fully two-phase plate-like $\eta+\epsilon$ increased from 0.09 to 0.50 with increase in alloy concentration from 3.1 to 6.3 at% Ag.

A plausible analysis was proposed to interpret the dependence of microstructural transitions on growth velocity in Zn–3.1 to 9.0 at% Ag alloys, that is, primary dendrites of ϵ in a matrix of peritectic $\eta\rightarrow$ two-phase plate-like $\eta + \epsilon$ with primary dendrites of $\epsilon\rightarrow$ fully two-phase plate-like $\eta + \epsilon$.

Acknowledgements

The authors wish to thank Professor H. Jones for his critical comments on our manuscript.

References

[1] Glardon R, Kurz W. J Cryst Growth 1981;51:283.
[2] Knoch KG, Reinsch B, Petzow G. Z Metallk 1994;85:350.
[3] Izumi T, Shiohara Y. J Mater Res 1992;7:16.
[4] Kerr HW, Kurz W. Int Mater Rev 1996;41:129.
[5] Cisse J, Kerr HW, Bolling GF. Metall Trans 1974;5:633.
[6] St John DH. Acta Metall Mater 1990;38:631.
[7] Lee JH, Verhoeven JD. J Cryst Growth 1994;144:353.
[8] Busse P, Meissen F. Scripta mater 1997;36:653.
[9] Vandyoussefi M, Kerr HW, Kurz W. Acta mater 2000;48:2297.
[10] Kurz W, Trivedi R. Metall Mater Trans 1996;27A:625.
[11] St John DH, Hogan LM. J Mater Sci 1984;19:939.
[12] Umeda T, Okane T, Kurz W. Acta mater 1996;44:4206.
[13] Boettinger WJ. Metall Trans 1974;5:2023.
[14] Ma D, Li Y, Ng SC, Jones H. Acta mater 2000;48:419.
[15] Xu W, Ma D, Feng YP, Li Y. Scripta mater 2001;44(4):631.
[16] Chalmers B. Physical metallurgy. New York: Wiley; 1959, p. 271–2.
[17] Flemings MC. In: Solidification processing. New York: McGraw–Hill; 1974:6–7.
[18] Massalski TB. Binary alloy phase diagrams. Metals Park, OH: American Society for Metals, 1986.
[19] Akdeniz MV, Wood JV. J Mater Sci 1996;31:545.
[20] Jackson KA, Hunt JD. Trans AIME 1966;236:1129.
[21] Hillert M. Solidification and casting of metals. London: The Metals Society; 1979:81-87.
[22] Laraia VJ, Heuer AH. Scripta metall mater 1991;25:2803.
[23] Brody HD, David SA. In: Solidification and casting of metals. London: The Metals Society; 1979:144-151.
[24] Kurz W, Fisher DJ. Fundamentals of solidification. 3rd ed. Aedermannsdorf (Switzerland): Trans Tech Publications, 1989.
[25] Gill SC, Kurz W. Acta metal mater 1993;41:3563.